Dynamics of a droplet driven by an internal active device

R. Kree, L. Rückert, and A. Zippelius*
Institut für Theoretische Physik, Universität Göttingen, Friedrich-Hund Platz 1, 37077 Göttingen, Germany

(Received 19 April 2020; accepted 9 February 2021; published 1 March 2021)

A liquid droplet, immersed into a Newtonian fluid, can be propelled solely by internal flow. In a simple model, this flow is generated by a collection of point forces, which represent externally actuated devices or model autonomous swimmers. We work out the general framework to compute the self-propulsion of the droplet as a function of the actuating forces and their positions within the droplet. A single point force, $\mathbf{F}$, with general orientation and position, $\mathbf{r}_0$, gives rise to both translational and rotational motion of the droplet. We show that the translational mobility is anisotropic and the rotational mobility can be nonmonotonic as a function of $|\mathbf{r}_0|$, depending on the viscosity contrast. Due to the linearity of the Stokes equation, superposition can be used to discuss more complex arrays of point forces. We analyze force dipoles, such as a stresslet, a simple model of a biflagellate swimmer and a rotlet, representing a helical swimmer, driven by an external magnetic field. For a general force distribution with arbitrary high multipole moments the propulsion properties of the droplet depend only on a few low order multipoles: up to the quadrupole for translational and up to a special octopole for rotational motion. The coupled motion of droplet and device is discussed for a few exemplary cases. We show in particular that a biflagellate swimmer, modeled as a stresslet, achieves a steady comoving state, where the position of the device relative to the droplet remains fixed. There are two fixed points, symmetric with respect to the center of the droplet. A tiny external force selects one of them and allows one to switch between forward and backward motion.

DOI: 10.1103/PhysRevFluids.6.034201

I. INTRODUCTION

Micro- and nanoscale medical robotics is a rapidly emerging area of research, which may open the way to many new and fascinating applications like precision surgery, directed drug delivery, microdiagnostic sensing, uptake of toxins, and many others (for recent reviews see [1,2]). A most important challenge on the way towards reliable biotechnological systems is to find bio-compatible, long-lasting, and precisely controllable methods of propulsion *in vivo*. Magnetically actuated helical micromotors on the 10-μm length scale, which are driven and controlled by external fields, provide a promising example. They have been used for important manipulations of soft materials, in particular for steerable locomotion in small droplets, for the actuation of human B lymphocytes and the assembly or disassembly of complexes of droplets and cells [3]. Furthermore, they have already been actuated in the peritoneal cavity of a mouse [4] for deep tissue analysis. Another promising technique is the biohybrid actuation, which uses molecular motors of biological systems as the propulsion mechanism. The big advantage of this approach is that fuel is provided by the surrounding biofluid, and these motors are highly optimized to convert the chemical energy into three-dimensional propulsion [5,6].

*kree@theorie.physik.uni-goettingen.de

In many aspects of biohybrid systems can we profit from copying evolutionary optimized designs from natural biological systems. In the case of self-propulsion [7], the design of artificial swimmers is inspired by biological microswimmers, such as algae, bacteria, and eukaryotic cells. Many of these have special organelles, e.g., flagellae or cilia, to propel the microorganism. However, swimming without specialized organelles is also found in nature. In the present paper, we want to explore possibilities of actuating a soft droplet by small internal motors, which either are externally driven or operate autonomously.

The motion of a passive particle in the presence of a rigid cavity was first considered by Oseen, who solved the Stokes equation for the flow field of a point force outside a spherical cavity [8]. Several extensions of Oseen's work have been obtained [9,10] and other geometries, such as plane walls and cylinders, have been considered. For a more recent exposition, see [11,12]. A Stokeslet near a spherical viscous drop was first considered by Fuentes *et al.* [13,14]. They solved the mobility problem for both the axisymmetric case [13] as well as motion perpendicular to the line connecting the centers [14]. Further solutions in terms of simple image systems have been constructed for point rotlets and point sources in [15]. Recently the oscillatory motion of a particle inside an elastic cavity was discussed [16,17]. Such a cavity is thought to model a vesicle that is enclosed by a membrane with shear and bending resistivity. Whereas the early works focused on colloidal suspensions [18,19], more recently active devices, such as squirmers inside a droplet, acquired attention. In [20], the locomotion of a spherical squirmer encapsulated inside a droplet of comparable size suspended in another viscous fluid has been studied. The authors show that the encaged swimmer can propel the droplet, and in some situations both remain in a stable coswimming state. In [21], the coswimming of a squirmer in a droplet with a nonuniform surface tension was studied. The latter provides an additional mechanism for self-propulsion and can increase or decrease both velocities, that of the squirmer and that of the droplet. Both papers [20,21] consider only axisymmetric configurations, resulting in translations.

Here we consider a spherical droplet that is immersed in an ambient Newtonian fluid and actuated by small internal motors. Our focus is the propulsion of the droplet due to an internal active device. We assume the device to be small as compared to the droplet and hence model it by a collection of point forces [22]. In contrast to [20,21], we consider asymmetric configurations and compute both the linear and rotational velocity of the droplet generated by point forces. Quantitative results are obtained for both cases, an autonomous force- and torque-free swimmer and an externally actuated device. In the next section (Sec. II) we introduce the model and we obtain its analytical solution in Sec. III. We present results for a single point force, representing an externally driven device, as well as for a dipolar and a quadrupolar force configuration, representing autonomous swimmers in Sec. IV. The coupled dynamics of droplet and device is discussed for exemplary cases in Sec. V. Conclusions are presented in Sec. VI; details of the analytical calculations are deferred to the Appendices.

II. MODEL

We want to study the propulsion of a droplet, which is driven by a device, which is either controlled externally or autonomous. The droplet is assumed to be spherical of radius R and consists of an incompressible Newtonian fluid with viscosity η^-. It is immersed into an ambient Newtonian fluid of viscosity η^+ which is at rest in the laboratory frame. The two fluids are assumed to be completely immiscible and of the same density ρ, so that the droplet is neutrally buoyant.

For small Reynolds number, the flow field created by the moving device can be calculated from Stokes's equation

$$\nabla \cdot \boldsymbol{\sigma} = \eta \nabla^2 \mathbf{v} - \nabla p = -\mathbf{f}, \tag{1}$$

supplemented by the incompressibility condition $\nabla \cdot \mathbf{v} = 0$. The viscosity η in Eq. (1) jumps between η^+ and η^- across the boundary of the droplet. The viscous stress tensor $\boldsymbol{\sigma}$ is given by its Cartesian components $\sigma_{ij} = -p\delta_{ij} + \eta(\partial_i v_j + \partial_j v_i)$, with the pressure p determined from the

incompressibility. The force density exerted by the active device is denoted by $\mathbf{f}$ and will be specified below. On the boundary of the droplet we assume continuity of the flow field $\mathbf{v}(\mathbf{r})$ and of the tangential stress, whereas the normal stress jumps due to the Laplace pressure $p_L = \gamma_0 \nabla \cdot \boldsymbol{n}$. The homogeneous surface tension is denoted by γ_0 and $\mathbf{n}$ is the normal of the droplet surface, which in general depends on θ and ϕ. Here we only consider the limit of high surface tension so that shape deformations can be neglected. The Laplace pressure is then given by $p_L = 2\gamma_0/R$ and the boundary condition for the normal stresses reads $\mathbf{e}_r \cdot (\boldsymbol{\sigma}_+ - \boldsymbol{\sigma}_-) = (2\gamma_0/R)\mathbf{e}_r$. Once the internal flow $\mathbf{v}$ has been computed, the linear and angular momentum of the droplet follow from

$$M\mathbf{v}_{CM} = \rho \int_V d^3x\, \mathbf{v}, \quad I\boldsymbol{\omega} = \rho \int_V d^3x\, \mathbf{r} \times \mathbf{v} \tag{2}$$

with total mass $M = \frac{4\pi\rho R^3}{3}$ and moment of inertia $I = \frac{8\pi\rho R^5}{15}$. Here the integral is over the volume V of the droplet.

We model the simplest externally controlled device by a point force:

$$\boldsymbol{f}(\mathbf{r}) = \mathbf{F}\delta(\mathbf{r} - \mathbf{r}_0). \tag{3}$$

Once the solution for the point force has been constructed, more general force distributions can be treated by superposition of the flow fields, because the Stokes equations are linear in $\mathbf{v}$. Of particular interest are force dipoles and force quadrupoles which can serve as models for an autonomous force-free swimmer. Another motivation for considering a point force stems from the following well-known fact [12]: The flow field of a moving sphere of radius a is correctly represented by a point force and a point quadrupole in unbounded space. Even though this result is not expected to hold for a sphere within a finite droplet, it may serve as an approximation provided the particle radius is small compared to all other length scales [22]. This point will be discussed in more detail in Sec. V.

III. ANALYTICAL SOLUTION

Our general strategy is to construct a special solution of the inhomogeneous equation and then add a homogeneous solution to match the boundary conditions. As a special solution of the inhomogeneous problem we can choose the classical Oseen tensor solution of a point force at position $\mathbf{r}_0$ in an unbounded fluid [12]:

$$8\pi\eta \mathbf{G}_{ij}(\mathbf{r} - \mathbf{r}_0) = \frac{1}{|\mathbf{r} - \mathbf{r}_0|}\delta_{ij} + \frac{(\mathbf{r} - \mathbf{r}_0)_i(\mathbf{r} - \mathbf{r}_0)_j}{|\mathbf{r} - \mathbf{r}_0|^3}. \tag{4}$$

However, the usual representation of this solution is not easy to match to boundary conditions on the surface of a sphere.

A. Expansion in vector spherical harmonics

Instead of expanding the Oseen tensor into solutions of the homogeneous Stokes equation, we prefer to construct the solution from the Stokes equation in terms of vector spherical harmonics (VSH) directly. Our choice of VSH is $\mathbf{Y}^{(0)}_{lm} = \mathbf{e}_r Y_{lm}$, $\mathbf{Y}^{(1)}_{lm} = r\nabla Y_{lm}$, and $\mathbf{Y}^{(2)}_{lm} = \mathbf{e}_r \times \mathbf{Y}^{(1)}_{lm}$. The vector spherical harmonics form a complete orthogonal set on the surface of a unit sphere with respect to the scalar product:

$$(\mathbf{h}, \mathbf{g}) = \int d\Omega\, \mathbf{h}^*(\Omega) \cdot \mathbf{g}(\Omega). \tag{5}$$

Not all of the $\mathbf{Y}^{(s)}_{lm} (s = 0, 1, 2)$ are normalized. While the $\mathbf{Y}^{(0)}_{lm}$ have norm 1, the $s = 1, 2$ fields have a norm of $(A^{(s)}_l)^{-1} = \ell(\ell + 1)$. For further properties of these functions we refer the reader to [23].

The expansion of the force density is explicitly given by

$$\mathbf{F}\delta(\mathbf{r}-\mathbf{r}_0)=\frac{\delta(r-r_0)}{r_0^2}\sum_{s=0}^{2}\sum_{l=0}^{\infty}\sum_{m=-l}^{l}f_{lms}(\Omega_0)\mathbf{Y}_{lm}^{(s)}(\Omega). \tag{6}$$

Here $f_{lms}(\Omega_0)=A_l^{(s)}[\mathbf{Y}_{lm}^{(s)}(\Omega_0)]^*\cdot\mathbf{F}$ and Ω_0 denotes the solid angle of $\mathbf{r}_0$, specifying its direction. The flow field and the pressure which are generated by the above point force are similarly expanded in VSH:

$$\boldsymbol{v}(\mathbf{r}|\mathbf{r}_0)=\sum_{s=0}^{2}\sum_{lm}v_{lms}(r,\mathbf{r}_0)\mathbf{Y}_{lm}^{(s)}(\Omega), \tag{7}$$

$$p(\mathbf{r}|\mathbf{r}_0)=\sum_{lm}p_{lm}(r,\mathbf{r}_0)Y_{lm}(\Omega). \tag{8}$$

The $\{v_{lms}\}$ and $\{p_{lm}\}$ are constructed by a superposition of a special solution of the inhomogeneous equation and the general solution of the homogeneous equation to satisfy the boundary conditions. This provides an exact analytic solution of the flow field of our model in terms of an infinite series. The applicability of this result may be limited by the rate of convergence of the series. For our purposes of calculating the propulsion velocities of the droplet [Eq. (2)], however, it proves to be very convenient, because the total momentum and angular momentum of the droplet are determined exclusively by the $l=1$ component. Inserting the expansion of $\mathbf{v}$ into Eq. (2) reveals (see [24])

$$\boldsymbol{v}_{CM}=\frac{3}{4\pi}\sum_m\int_{\partial V}d\Omega\; v_{1m0}(r=R,\mathbf{r}_0)Y_{1m}(\Omega)\mathbf{e}_r, \tag{9}$$

$$\boldsymbol{\omega}=-\frac{15}{8\pi R^5}\sum_m\int_V d^3r\; r^2\; v_{1m2}(r,\mathbf{r}_0)\nabla Y_{1m}(\Omega). \tag{10}$$

B. Solution inside the droplet

The solution outside of the droplet is standard, so that we concentrate here on the interior of the droplet. The homogeneous solutions to the Stokes equation in the interior of the droplet are well known and explicitly given by

$$v_{1m0}^{\mathrm{hom}}(r)=a_{lm}^{-}\left(\frac{r}{R}\right)^{\ell+1}+b_{lm}^{-}\left(\frac{r}{R}\right)^{\ell-1}, \tag{11}$$

$$v_{lm2}^{\mathrm{hom}}(r)=c_{lm}^{-}\left(\frac{r}{R}\right)^{\ell}. \tag{12}$$

The constraint of incompressibility determines v_{lm1}^{hom}.

The difficult part is the construction of a special solution of the inhomogeneous equation, given the point force singularity in the interior of the droplet. The first step is to decompose the interior of the droplet into a sphere with radius $r\leqslant r_0$ and the enclosing space, a spherical shell, defined by $r_0\leqslant r\leqslant R$ (see Fig. 1). In the inner space ($r\leqslant r_0$), we use the solutions of the Stokes equation which are regular at the origin. In the outer shell ($r_0\leqslant r\leqslant R$), but still within the droplet, the flow is represented by both solutions of the Stokes equation, the ones which are regular at the origin and the other ones which are regular at infinity.

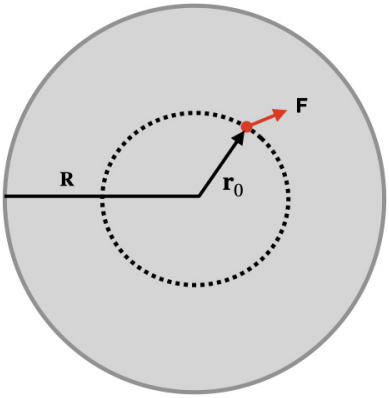

FIG. 1. Decomposition of the interior of the droplet into an inner sphere $r \leqslant r_0$ and an outer shell $r_0 \leqslant r \leqslant R$, used for the construction of the flow field generated by a point force $\mathbf{F}\delta(\mathbf{r}-\mathbf{r}_0)$ in the interior.

Inserting the expansions [Eqs. (6)–(8)] into Eq. (1), the Stokes equation is converted into three ordinary differential equations for the $\{v_{lms}(r)\}$ and $\{p_{lm}(r)\}$:

$$\eta\begin{pmatrix} \left(\frac{d^2}{dr^2}+\frac{2}{r}\frac{d}{dr}\right)-\frac{[2+l(l+1)]}{r^2} & \frac{2l(l+1)}{r^2} & 0 \\ \frac{2}{r^2} & \left(\frac{d^2}{dr^2}+\frac{2}{r}\frac{d}{dr}\right)-\frac{l(l+1)}{r^2} & 0 \\ 0 & 0 & \left(\frac{d^2}{dr^2}+\frac{2}{r}\frac{d}{dr}\right)-\frac{l(l+1)}{r^2} \end{pmatrix}\begin{pmatrix} v_{lm0} \\ v_{lm1} \\ v_{lm2} \end{pmatrix}$$
$$=\begin{pmatrix} \frac{dp_{lm}}{dr} \\ \frac{p_{lm}}{r} \\ 0 \end{pmatrix}-\frac{\delta(r-r_0)}{r_0^2}\begin{pmatrix} f_{lm0} \\ f_{lm1} \\ f_{lm2} \end{pmatrix}. \tag{13}$$

(In the following we suppress the dependence on $\mathbf{r}_0$ to keep the notation transparent.) The above system of equations decouples into a 2×2 block for the nonchiral flow, generated by f_{lm0} and f_{lm1}, and a single equation for the chiral flow, generated by f_{lm2}. Hence chiral and nonchiral flow can be discussed separately. We choose to first solve for the chiral part because it is simpler and allows us to fully explain our method of solution.

C. Chiral flow

We take $f_{lm0}=f_{lm1}=0$ and concentrate on the rotational flow:

$$\boldsymbol{v}(\mathbf{r})=\sum_{l,m} v_{lm2}\,\mathbf{r}\times\nabla Y_{lm}$$

where v_{lm2} is the solution of

$$\eta^{-}\left(\frac{d^2}{dr^2}+\frac{2}{r}\frac{d}{dr}-\frac{l(l+1)}{r^2}\right)v_{lm2}=-\frac{f_{lm2}}{r_0^2}\delta(r_0-r). \tag{14}$$

A special solution of this equation is constructed with help of the inner and outer solutions with respect to the position of the point force $\mathbf{r}_0$. We thus make the ansatz

$$\frac{v_{lm2}^{\mathrm{inh}}}{R}=K_{lm}\left(\frac{r}{R}\right)^{\ell}\Theta(r_0-r)+G_{lm}\left(\frac{R}{r}\right)^{\ell+1}\Theta(r-r_0)$$

[where $\Theta(x) = 1$ for $x > 0$ and $\Theta(x) = 0$ for $x < 0$ denotes the Heaviside function] and plug it into Eq. (14) to determine the coefficients:

$$G_{lm} = \frac{f_{lm2}}{\eta^- R^2(2l+1)}\left(\frac{r_0}{R}\right)^l, \quad K_{lm} = \frac{f_{lm2}}{\eta^- R^2(2l+1)}\left(\frac{R}{r_0}\right)^{l+1}.$$

Thereby we have constructed a special solution to the inhomogeneous equation (14). We now add the homogeneous solution, Eq. (12),

$$v_{lm2} = c^-_{lm}\left(\frac{r}{R}\right)^\ell + v^{\text{inh}}_{lm2}, \tag{15}$$

to fulfill the boundary conditions. Note that in the shell $r_0 \leqslant r \leqslant R$ we indeed need both solutions for the flow field, namely, those which are regular at the origin and those which are regular at infinity.

Two boundary conditions at the surface of the droplet have to be fulfilled: continuity of the flow and of the tangential stresses. The internal flow has been derived above and the exterior (chiral) flow is given by $v^+_{lm2} = c^+_{lm}(\frac{R}{r})^{l+1}$. The first boundary condition thus reads

$$c^+_{lm} = c^-_{lm} + \frac{f_{lm2}}{R\eta^-(2l+1)}\left(\frac{r_0}{R}\right)^l. \tag{16}$$

The second boundary condition requires that the surface of the droplet be force free. We define the surface tractions $\mathbf{t} = \mathbf{e}_r \cdot \boldsymbol{\sigma}|_{r=R}$ and their chiral components $t_{lm2} = \frac{1}{2}\int d\Omega\, \mathbf{t} \cdot [\mathbf{Y}^{(2)}_{lm}(\Omega)]^*$. Given the interior and exterior flow fields, the computation of the tractions is straightforward: $t_{lm2} = \eta(\frac{d}{dr} - \frac{1}{r})v_{lm2}$. Continuity, $t^+_{lm2} = t^-_{lm2}$ implies

$$c^+_{lm}(2+l)\eta^+ = -c^-_{lm}(l-1)\eta^- + f_{lm2}\frac{l+2}{(2l+1)}\frac{r_0^l}{R^{l+1}}. \tag{17}$$

These two equations (16) and (17) determine the free coefficients completely:

$$c^+_{lm} = \frac{f_{lm2}}{R\eta^+}\left(\frac{r_0}{R}\right)^l \frac{1}{2+l+\lambda(l-1)}, \quad c^-_{lm} = \frac{f_{lm2}}{R\eta^+}\frac{l+2}{2l+1}\left(\frac{r_0}{R}\right)^l \frac{1-1/\lambda}{2+l+\lambda(l-1)}.$$

Here we have introduced the viscosity contrast $\lambda = \eta^-/\eta^+$.

The rotational velocity $\boldsymbol{\omega}$ is determined exclusively by the $\ell = 1$ component of the flow [Eq. (10)], which is given explicitly by

$$v_{1m2}(r, \mathbf{r}_0) = \frac{f_{1m2}(\Omega_0)}{3\eta^-}\left[(\lambda-1)\frac{r r_0}{R^3} + \Theta(r-r_0)\frac{r_0}{r^2} + \Theta(r_0-r)\frac{r}{r_0^2}\right].$$

Substituting this result into Eq. (10) yields the rotational velocity of the droplet:

$$\boldsymbol{\omega} = \frac{\mathbf{r}_0 \times \mathbf{F}}{16\pi\eta^- R^3}\left[2\lambda + 3\left(1 - \left(\frac{r_0}{R}\right)^2\right]\right], \tag{18}$$

which will be discussed in Sec. IV A.

D. Nonchiral flow

Next we consider the nonchiral flow with $f_{lm2} = 0$. The coupled equations for the two components of the flow v_{lm0}, v_{lm1} can be decoupled using the constraint of incompressibility,

$$\frac{dv_{lm0}}{dr} + \frac{2}{r}v_{lm0} - \frac{l(l+1)}{r}v_{lm1} = 0, \tag{19}$$

resulting in a single equation for v_{lm0}:

$$\eta\left(\frac{d^2}{dr^2} + \frac{4}{r}\frac{d}{dr} + \frac{2-l(l+1)}{r^2}\right)v_{lm0} = \frac{dp_{lm}}{dr} - \frac{f_{lm0}}{r_0^2}\delta(r-r_0). \tag{20}$$

In order to solve it, we first have to compute the pressure, again using the constraint of incompressibility, $\nabla^2 p = \nabla \cdot \mathbf{f}$, to obtain

$$\frac{d^2 p_{lm}}{dr^2} + \frac{2}{r}\frac{dp_{lm}}{dr} - \frac{l(l+1)}{r^2} p_{lm} = \frac{f_{lm0}}{r_0^2}\frac{d}{dr}\delta(r-r_0) + \frac{2f_{lm0}}{r_0^3}\delta(r-r_0) - \frac{l(l+1)f_{lm1}}{r_0^3}\delta(r-r_0). \tag{21}$$

A special solution of this equation is constructed with help of the inner and outer solutions with respect to the position of the point force $\mathbf{r}_0$. We thus use the ansatz,

$$p_{lm}^{\mathrm{inh}}(r) = A_{lm}\left(\frac{r}{R}\right)^{\ell}\Theta(r_0 - r) + B_{lm}\left(\frac{R}{r}\right)^{\ell+1}\Theta(r - r_0)\,, \tag{22}$$

plug it into Eq. (21), and find for the coefficients A_{lm} and B_{lm}

$$A_{lm} = \frac{1}{r_0^2}\frac{\ell(\ell+1)f_{lm1} - (\ell+1)f_{lm0}}{2\ell+1}\left(\frac{R}{r_0}\right)^{\ell}, \tag{23}$$

$$B_{lm} = \frac{1}{r_0^2}\frac{\ell(\ell+1)f_{lm1} + \ell f_{lm0}}{2\ell+1}\left(\frac{r_0}{R}\right)^{\ell+1}. \tag{24}$$

Note that the pressure is discontinuous at r_0, as it has to be due to the singularities on the right hand side of Eq. (21).

If this solution for the pressure is substituted into Eq. (20), one observes that the contributions involving $\delta(r - r_0)$ cancel and one obtains the following equation for v_{lm0}:

$$\eta^{-}\left(\frac{d^2}{dr^2} + \frac{4}{r}\frac{d}{dr} + \frac{2 - l(l+1)}{r^2}\right)v_{lm0} = \frac{\ell}{r}A_{lm}\left(\frac{r}{R}\right)^{\ell}\Theta(r_0 - r) - \frac{\ell+1}{r}B_{lm}\left(\frac{R}{r}\right)^{\ell+1}\Theta(r - r_0). \tag{25}$$

The equation is solved by linear combinations of the inner and outer solutions as detailed in Appendix A. Once a special solution of the inhomogeneous equation has been constructed, we subsequently add the general solution of the homogeneous equations. This leaves us with four sets of yet unknown coefficients $\{a_{lm}^{-}, b_{lm}^{-}\}$ for the flow inside the droplet and $\{a_{lm}^{+}, b_{lm}^{+}\}$ for the exterior flow. These are determined by four boundary conditions, two resulting from continuity of the flow at the droplet's surface and two from the condition that the interface be force free. These four equations are given and solved in Appendix B [see Eqs. (B3)–(B6)].

IV. RESULTS

The general formalism of the previous section allows us to give simple and exact expressions for the translational and rotational velocities of a droplet, which is driven by a configuration of point forces. This is the central finding of the present paper. In this section we first give basic results for the propulsion velocities $\mathbf{v}_{\mathrm{cm}}$ and $\boldsymbol{\omega}$ due to a single point force. All other configurations can be studied by linear superpositions of these velocities. As examples, we consider pairs of point forces, such as stresslets and rotlets, and a device made of three linearly arranged points (see Fig. 2). The examples have been chosen to provide crude approximations of biflagellate microorganisms and of helical magnetic swimmers. Finally, we discuss arbitrary configurations and show that only a few low order multipoles of the force distribution determine the propulsion velocities completely.

A. Single point force

First consider a single point force $\mathbf{f}(\mathbf{r}) = \mathbf{F}\delta(\mathbf{r} - \boldsymbol{r}_0)$, representing an externally driven device. Such a device gives rise to both translational and rotational motion of the droplet. For the center of

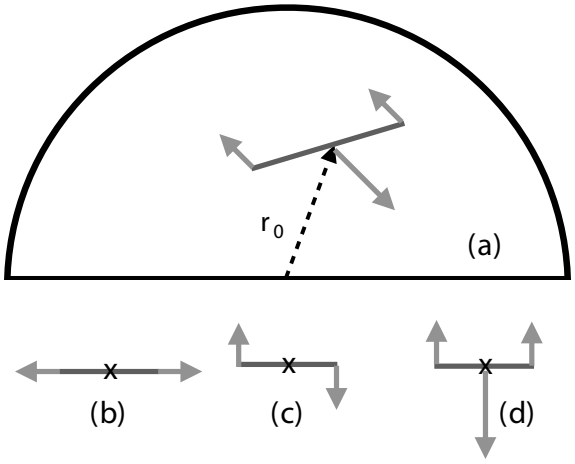

FIG. 2. (a) Upper half of the droplet with examples of devices of point forces at $\mathbf{r}_0$. (b) Stresslet. (c) Rotlet. (d) Quadrupolar device. The point forces are indicated by vectors.

mass velocity we find

$$\boldsymbol{v}_{\rm cm} = \frac{1}{4\pi\eta^+ R}\frac{1}{(3\lambda+2)}\Big[(2\lambda+3)\mathbf{F} - \Big(\frac{r_0}{R}\Big)^2(2\mathbf{F}-\mathbf{F}_{||})\Big] =: \boldsymbol{\mu}_t(\mathbf{r}_0)\cdot\mathbf{F}. \tag{26}$$

Here we have introduced the vector component of the force parallel to $\mathbf{r}_0$, $\mathbf{F}_{||} = (\mathbf{F}\cdot\mathbf{r}_0)\mathbf{r}_0/r_0^2$.

As expected, we find a linear relation between $\mathbf{v}_{\rm cm}$ and the externally applied force with, however, an *anisotropic* mobility tensor $\boldsymbol{\mu}_t$. In other words, the droplet does in general not move in the direction of the applied force. The mobility for a force parallel to $\mathbf{r}_0$ is always larger than the mobility for a force perpendicular to $\mathbf{r}_0$: $\mu_{\|} - \mu_{\perp} = \frac{1}{4\pi\eta^+ R}\frac{1}{3\lambda+2}(\frac{r_0}{R})^2$.

The angular velocity [Eq. (18)] is linearly related to the torque with respect to the center of the droplet: $\boldsymbol{\omega} = \mu_{\rm rot}(r_0)\,\mathbf{r}_0\times\mathbf{F}$. The rotational mobility $\mu_{\rm rot}$,

$$\mu_{\rm rot}(r_0) = \frac{1}{16\pi\eta^- R^3}\Big\{2\lambda+3\Big[1-\Big(\frac{r_0}{R}\Big)^2\Big]\Big\}, \tag{27}$$

is isotropic and decreasing with r_0 while the torque is increasing. This may lead to a nonmonotonic dependence of $\boldsymbol{\omega}(r_0)$. For example, a point force $\mathbf{F} = F\mathbf{e}_x$ located on the z axis at $\mathbf{r}_0 = z_0\mathbf{e}_z$ causes an angular frequency $\boldsymbol{\omega} = \omega(z_0)\mathbf{e}_y$, which takes on a maximum at $z^*/R = \sqrt{2\lambda+3}/3$, which is inside the droplet if $\lambda < 3$.

Rotation is prevented, if the torque with respect to the center of the droplet vanishes, i.e., if the force is parallel to $\mathbf{r}_0$. Choosing $\mathbf{F} = F\mathbf{e}_z$ and $\mathbf{r} = z_0\mathbf{e}_z$ the droplet moves in the z direction with a translational mobility of the form

$$\mu(z_0) = \mu_{\rm HR} + \frac{1}{4\pi\eta^+ R}\frac{1-\big(\frac{z_0}{R}\big)^2}{2+3\lambda}, \tag{28}$$

where $\mu_{\rm HR} = (1/2\pi\eta^+ R)[(\lambda+1)/(2+3\lambda)]$ is the classical result of Hadamard and Rybczynski for a spherical droplet moving with prescribed velocity [12]. The correction vanishes, if the singularity is moved to the surface of the droplet $z_0 \to R$. In other words the inner sphere in Fig. 1 fills the whole droplet and the outer shell vanishes. For a general position of the point force $\mu(z_0) \geqslant \mu_{\rm HR}$.

B. Force dipoles

We are interested in the propulsion of a droplet, driven by an encapsulated, autonomous swimmer. These are frequently modeled as force dipoles $\mathbf{f}(\mathbf{r}) = \mathbf{F}\delta(\mathbf{r}-\mathbf{r}^+) - \mathbf{F}\delta(\mathbf{r}-\mathbf{r}^-)$ with $\mathbf{r}^\pm = \mathbf{r}_0 \pm \mathbf{d}/2$ (see Fig. 2). The total force vanishes, but there is in general a nonzero torque. The propulsion velocities of the droplet driven by a force dipole are obtained from Eqs. (26) and (18) by superposition. The results for a general position and orientation of the point forces are given in Appendix C. Here we only discuss two special cases, the stresslet and the rotlet which have been suggested as simple models for microswimmers.

The simplest example of a fully autonomous device is a *stresslet*-like force pair characterized by $\mathbf{F} = F\mathbf{d}/d$ [see Fig. 1(b)]. This may be considered as a crude approximation of a biflagellate microorganism [25] with a thrust $\mathbf{F}$ exerted by flagella and balanced by the viscous drag $-\mathbf{F}$ of the cell body. Note that the symmetric configuration studied here would not lead to self-propulsion of the device in free space.

The translational velocity of the droplet driven by a stresslet is given by

$$\boldsymbol{v}_{\rm cm} = \frac{Fd}{4\pi R^3(3\eta^- + 2\eta^+)}\left(\mathbf{r}_0 - 3\frac{\mathbf{d}\cdot\mathbf{r}_0}{d^2}\mathbf{d}\right).$$

The mobility is anisotropic and vanishes, if either η^+ or η^- becomes very large. Although the stresslet's intrinsic torque is zero, it will generate rotational motion of the droplet with

$$\boldsymbol{\omega} = -\frac{3}{8\pi\eta^- R^5}(\mathbf{r}_0\cdot\mathbf{d})\,(\mathbf{r}_0\times\mathbf{F}).$$

This angular velocity is independent of the exterior viscosity; it only vanishes if $\mathbf{d}$ is perpendicular to $\mathbf{r}_0$ or if $\mathbf{F}$ is parallel to $\mathbf{r}_0$.

A *rotlet*-like force pair $\mathbf{F} \perp \mathbf{d}$ [see Fig. 1(c)] may be considered as a first approximation to a helical magnetic swimmer driven by a rotating magnetic field [3,26] and exerting a finite torque on the fluid. The propulsion velocities are easily read off from Eqs. (C11) and (C12) and show that the droplet is not only rotated but also translated by this force pair. If, for example, $\mathbf{d} \,||\, \boldsymbol{e}_x$ and $\mathbf{F} \,||\, \boldsymbol{r}_0 = z_0\boldsymbol{e}_z$ the droplet will move in the x direction with speed $v_{\rm cm} = Fdz_0/[4\pi R^3(3\eta^- + 2\eta^+)]$.

Pointlike force dipoles are included in the above results by taking the limit $d \to 0$ while keeping the dipole strength Fd fixed. The propulsion velocities for general orientations of $(\mathbf{r}_0, \mathbf{d}, \mathbf{F})$ are given in Appendix C.

C. Quadrupolar autonomous device

As a last example of simple point force configurations consider a slightly refined model of a biflagellate microorganism characterized by $\mathbf{f}(\mathbf{r}) = 2\mathbf{F}\delta(\mathbf{r}-\mathbf{r}_0) - \mathbf{F}\delta(\mathbf{r}-\mathbf{r}_0-\mathbf{d}) - \mathbf{F}\delta(\boldsymbol{r}-\boldsymbol{r}_0+\mathbf{d})$ [see Fig. 1(d)]. Here the two flagellae are described as separate, symmetrically arranged point forces [27]. The device is *fully autonomous*, because both the total force and the torque with respect to the point $\mathbf{r}_0$ vanish. The propulsion velocities become

$$\mathbf{v}_{\rm cm} = \frac{1}{4\pi\eta^+ R^3}\frac{1}{3\lambda+2}[4d^2\mathbf{F} - 2(\mathbf{d}\cdot\mathbf{F})\mathbf{d}] \tag{29}$$

and

$$\boldsymbol{\omega} = \frac{3}{8\pi\eta^- R^5}[(2\boldsymbol{r}_0\cdot\mathbf{d})(\mathbf{d}\times\mathbf{F}) + d^2(\boldsymbol{r}_0\times\mathbf{F})]. \tag{30}$$

Note that unlike a single point force or a force pair the translation velocity of the three point device is independent of the position $\mathbf{r}_0$ of the configuration in the droplet's interior. The droplet is translated without rotation if $\mathbf{F} \,||\, \boldsymbol{r}_0$ and $\mathbf{d} \perp \boldsymbol{r}_0$ hold.

D. Droplet driven by a general configuration of point forces

It is straightforward to generalize the results of the previous subsection to arbitrary configurations $\mathbf{f}(\mathbf{r}) = \sum_{\nu=1}^{M} \mathbf{F}^{(\nu)} \delta(\boldsymbol{r} - \boldsymbol{r}^{(\nu)})$ with $\mathbf{r}^{(\nu)} = \boldsymbol{r}_0 + \mathbf{d}^{(\nu)}$. The point $\boldsymbol{r}_0$, which here appears as an arbitrary marking of the position of the device, may acquire a physical meaning in more detailed models as will be discussed in Sec. V. Superposition of the contributions of point forces gives the propulsion velocities

$$\boldsymbol{v}_{\mathrm{cm}} = \frac{1}{4\pi\eta^{+}R} \frac{1}{3\lambda + 2} \tag{31}$$

$$\left[(2\lambda + 3)\mathbf{F}_M - \sum_{\nu=1}^{M} \left(\frac{r^{(\nu)}}{R} \right)^2 \left(2\mathbf{F}^{(\nu)} - \mathbf{F}_{||}^{(\nu)} \right) \right] \tag{32}$$

and

$$\boldsymbol{\omega} = -\frac{1}{16\pi\eta^{-}R^3} \left[(2\lambda + 3)(\boldsymbol{N}_M + \boldsymbol{r}_0 \times \mathbf{F}_{\mathbf{M}}) - 3 \sum_{\nu} \left(\frac{r^{(\nu)}}{R} \right)^2 \boldsymbol{r}^{(\nu)} \times \mathbf{F}^{(\nu)} \right], \tag{33}$$

which are determined by only a few low order multipoles. It is easily seen by inserting $\boldsymbol{r}^{(\nu)} = \boldsymbol{r}_0 + \mathbf{d}^{(\nu)}$ into Eqs. (31) and (33) that $\boldsymbol{v}_{\mathrm{cm}}$ is completely fixed by the total force $\mathbf{F}_M = \sum_{\nu=1}^{M} \mathbf{F}^{(\nu)}$, the second rank tensor of force dipole moments $\mathbf{d} = \sum_{\nu} \mathbf{d}^{(\nu)} \mathbf{F}^{(\nu)}$ (including the total torque $\boldsymbol{N}_M = \sum_{\nu=1}^{M} \mathbf{d}^{(\nu)} \times \mathbf{F}^{(\nu)}$), and the third rank tensor of quadrupole moments $\mathbf{Q} = \sum_{\nu} \mathbf{d}^{(\nu)} \mathbf{d}^{(\nu)} \boldsymbol{F}^{(\nu)}$. For the angular velocity, $\boldsymbol{\omega}$, a special octopole moment $\boldsymbol{W} = \sum_{\nu} (\mathbf{d}^{(\nu)} \cdot \mathbf{d}^{(\nu)})\, \mathbf{d}^{(\nu)} \mathbf{F}^{(\nu)}$ is needed in addition. Therefore different distributions of internal forces may generate the same propulsion velocities. In particular, if the configuration is autonomous and its dipole moment vanishes, the translation velocity is independent of the position $\boldsymbol{r}_0$ (the three point device of the previous subsection is a simple example). If in addition $\mathbf{Q} = \mathbf{0}$ but $\boldsymbol{W}$ is finite then $\boldsymbol{v}_{\mathrm{cm}} = \mathbf{0}$ and the droplet is only rotated. All higher order multipole moments beyond the octopole do not generate any propulsion of the droplet.

V. COUPLED DYNAMICS OF DEVICE AND DROPLET

So far we have discussed snapshots of a droplet and a device, the latter being treated as an assembly of point forces. The motion of a real device within the droplet depends upon the details of its material properties, its structure, and its internal dynamics. A discussion of the general case is beyond the scope of this paper. In the following, we illustrate the use of our results to determine the coupled evolution of the droplet and devices consisting of small spherical beads. We consider a single bead dragged by an external force and a simple steering problem of a biflagellate model.

When we integrate the device velocity to determine its trajectory, we assume that the droplet retains its spherical shape. As the flow field on the interface contains shape-changing components, these have to be counteracted by large surface tension, which prevents any changes in area, i.e., we have to assume a sufficiently small capillary number [28].

A. Small bead dragged by an external force

In Sec. IV A we have computed the propulsion of the droplet by a device consisting of a single point force in the interior. In order to derive an approximate velocity for the device, we now replace the point force by a spherical particle of radius a which is dragged along the z axis by an external force $\mathbf{F}^{\mathrm{ext}} = F^{\mathrm{ext}} \boldsymbol{e}_z$. The current position of the center of the sphere is $\boldsymbol{r}_0 = z_0 \boldsymbol{e}_z$. In free space its velocity is given by Stokes's law as $\boldsymbol{U}_{\mathrm{sphere}} = \mathbf{F}^{\mathrm{ext}}/(6a\pi\eta^{-}) = \mu_0 \mathbf{F}^{\mathrm{ext}}$. In the droplet the moving sphere causes a response flow $\boldsymbol{v}^{(a)}(\boldsymbol{r}|\boldsymbol{r}_0)$ due to the interface and the device velocity can be obtained

from Faxén's law in the explicit form

$$\boldsymbol{U}_{\text{sphere}} = \mu_0 \mathbf{F}^{\text{ext}} + \left(1 + \frac{a^2}{6}\nabla^2\right)\boldsymbol{v}^{(a)}(\boldsymbol{r}_0|\boldsymbol{r}_0), \tag{34}$$

provided the response flow, $\boldsymbol{v}^{(a)}(\boldsymbol{r}|\mathbf{r}_0)$, is known in the vicinity of $\boldsymbol{r} \sim \boldsymbol{r}_0$. For a small sphere ($a \ll 1$), with distance $D \gg a$ from the interface, we approximate the flow it generates at the interface by that of its leading multipole, i.e., the flow due to a point force $\mathbf{F}^{\text{ext}}$, calculated in Appendix A. Furthermore, the internal flow is determined by all ℓ components in the expansion (7) and not just the $\ell = 1$ component which determines the instantaneous propulsion. The flow field with $\ell > 1$, in general, induces shape deformations which we assume to be small due to strong surface tension. Since we do not include the shape conserving terms explicitly, our calculation of the internal flow is only approximate and this may limit the computation of trajectories to small times.

For the axially symmetric structure of the device, $\mathbf{r}_0 = z_0\mathbf{e}_z$ and $\mathbf{F} = F\mathbf{e}_z$, the calculations simplify considerably. The response flow is parallel to the z axis $\mathbf{v}^{(a)}(\mathbf{r}_0|\mathbf{r}_0) = v^{(a)}(z_0)\mathbf{e}_z$ and explicitly given by

$$v^{(a)}(z_0) = \sum_{l=1}^{\infty}\left(\frac{2l+1}{4\pi}\right)^{1/2}\left[a_{l0}^{-}\left(\frac{z_0}{R}\right)^{l+1} + b_{l0}^{-}\left(\frac{z_0}{R}\right)^{l-1}\right]. \tag{35}$$

Here a_{lm}^{-} and b_{lm}^{-} are defined in Eqs. (11) and (A2).

Comparing the device velocity to the droplet velocity, as given in Eq. (26), we find that $\mathbf{U}_{\text{device}} - \mathbf{v}_{\text{cm}}$ is always positive for a device in the interior of the droplet, i.e., $a + |z_0| < R$. It is minimal for the device in the center of the droplet and grows as the device moves towards the interface. For an illustrative example with particle radius $a = 0.05$ and a viscosity contrast $\lambda = 30$, the difference is a few percent.

B. Externally guided biflagellate

Given the above approximate velocity of the device, we are now looking for a dynamic state, in which the droplet and the encapsulated device (the swimmer) move with the *same* velocity. Otherwise, if the swimmer is faster or slower than the droplet, it will move out of the droplet and the composite system will be unstable. To achieve a stationary, comoving state one needs two driving mechanisms: the activity of an autonomous swimmer and an external steering force. The latter is acting on the device and has to be adjusted appropriately to the swimming activity in order to produce a stable state with the same velocities for droplet and encapsulated device and hence fixed relative position of the two.

As a simple example, consider a variant of the three point biflagellate model, which was introduced in Sec. IV B. Here the device consists of a spherical particle of radius $a < d$ centered at $z_0\boldsymbol{e}_z$ and flagella (with negligible hydrodynamic resistance) exerting point forces $\pm F\boldsymbol{e}_z$ at $\mathbf{r}^{\pm} = (z_0 \pm d)\boldsymbol{e}_z$. The point forces add up to zero. An additional force $\mathbf{F}^{\text{ext}} = F^{\text{ext}}\boldsymbol{e}_z$ is acting on the sphere to guide the device (see Fig. 3). More explicitly, the force dipole models the swimming activity of the device and the external force will be adjusted so that the velocity of the droplet coincides with the velocity of the device.

In the absence of the sphere the point forces create a flow $\tilde{\boldsymbol{v}}$, which consists of a sum of Stokeslets and the corresponding response flows $\boldsymbol{v}^{(\pm)}(\boldsymbol{r}|\boldsymbol{r}^{\pm})$ due to the droplet interface, i.e.,

$$\tilde{\boldsymbol{v}}(\boldsymbol{r}) = [\boldsymbol{G}(\boldsymbol{r} - \boldsymbol{r}^{+}) - \boldsymbol{G}(\mathbf{r} - \boldsymbol{r}^{-})] \cdot \mathbf{F} + \boldsymbol{v}^{(+)}(\boldsymbol{r}|\boldsymbol{r}^{+}) + \boldsymbol{v}^{(-)}(\boldsymbol{r}|\boldsymbol{r}^{-}). \tag{36}$$

Here $\boldsymbol{G}$ denotes the Oseen tensor [Eq. (4)]. If we now add the spherical particle at position $\boldsymbol{r}_0$, it will be advected by the flow $\tilde{\boldsymbol{v}}(\boldsymbol{r}_0)$. At $\boldsymbol{r} = \boldsymbol{r}_0$ the first term on the right hand side vanishes, because $\boldsymbol{G}$ is an even function of its argument. Including the Faxén correction, this flow drives the sphere with

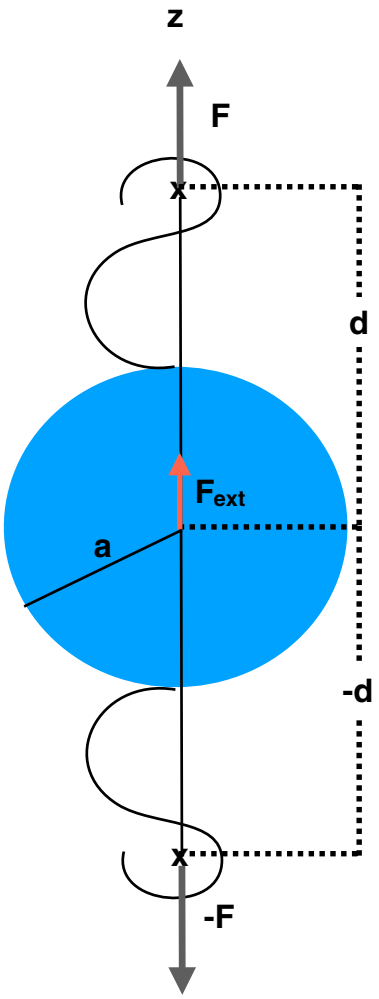

FIG. 3. Biflagellate swimmer, modeled by a small sphere with an attached stresslet and subject to an external force $\mathbf{F}^{\text{ext}}$, which will be tuned to the swimming activity to achieve a stable comoving state of droplet and device. All length scales are assumed to be small as compared to the droplet's radius.

velocity

$$\boldsymbol{U}_{\text{stresslet}} = \left(1 + \frac{a^2}{6}\nabla^2\right)[\boldsymbol{v}^{(+)}(\boldsymbol{r}_0|\boldsymbol{r}^+) + \boldsymbol{v}^{(-)}(\boldsymbol{r}_0|\boldsymbol{r}^-)]. \tag{37}$$

In addition to the swimming activity, as described by the force dipole, we now turn on an external steering force $\mathbf{F}^{\text{ext}}$, so that the velocity of the device is given by the sum of Eqs. (34) and (37), $\boldsymbol{U}_{\text{device}} = \boldsymbol{U}_{\text{sphere}} + \boldsymbol{U}_{\text{stresslet}}$. This velocity contains the response flow $\boldsymbol{v}^{(a)}$ due to the particle, which we replace by the response flow of the point force $\mathbf{F}^{\text{ext}}$ as explained in the previous subsection. As the flow is smooth at $\boldsymbol{r}_0$, we can drop the derivative term $\propto a^2\nabla^2$ to obtain the device velocity to leading order in a:

$$\boldsymbol{U}_{\text{device}} = \mu_0\mathbf{F}^{\text{ext}} + \boldsymbol{v}^{(+)}(\boldsymbol{r}_0|\boldsymbol{r}^+) + \boldsymbol{v}^{(-)}(\boldsymbol{r}_0|\boldsymbol{r}^-) + \boldsymbol{v}^{(a)}(\boldsymbol{r}_0|\boldsymbol{r}_0). \tag{38}$$

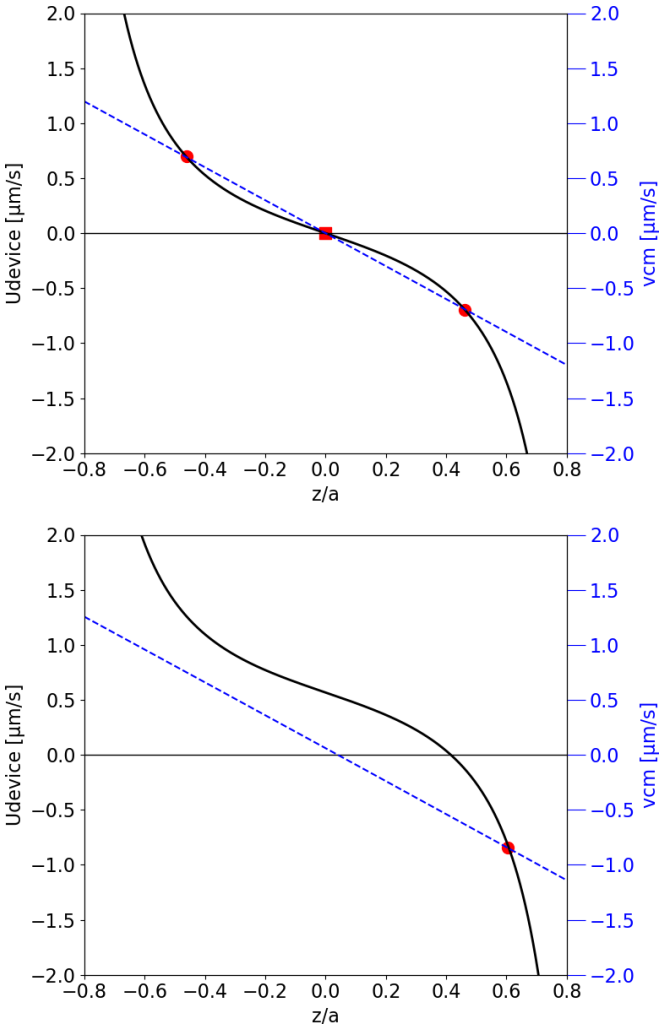

FIG. 4. Device velocity $\boldsymbol{U}_{\text{device}}$ (solid line) and droplet velocity (dashed line) generated by the device described in the main text with point forces F of 1 pN at a distance $d = 2$ μm from a bead with radius 1 μm, in a droplet of radius 50 μm. Top: Without steering force $F^{\text{ext}} = 0$. Stable fixed points are marked by circles; unstable fixed points are marked by squares. Bottom: With $F^{\text{ext}} = 0.001$ pN. The viscosity contrast is $\lambda = 5$ and contributions up to $l = 50$ are taken into account. No visible changes appear if contributions up to $l = 100$ are added.

The steering force can now be used to control the velocity of the device relative to the droplet velocity. The latter is obtained from Eq. (26) by superposition of the three point forces and is explicitly given by

$$\boldsymbol{v}_{\text{cm}} = \frac{1}{4\pi\eta^{+}R}\frac{1}{3\lambda+2}\left\{\left[2\lambda+3-\left(\frac{z_0}{R}\right)^2\right]F^{\text{ext}}\boldsymbol{e}_z - 4\frac{dz_0}{R}F\boldsymbol{e}_z\right\}. \tag{39}$$

The relative velocity $\boldsymbol{U}_{\text{device}} - \boldsymbol{v}_{\text{cm}}$ is shown in Fig. 4. If $F^{\text{ext}} = 0$ [Fig. 4(a)] there are two off-center stable fixed points of the one-dimensional motion of the biflagellate, whereas the center of the sphere

is an unstable fixed point. With a tiny external force one can select a stable fixed point [Fig. 4(b)], which makes it possible to switch between forward and backward motion along the z axis. With increasing F^{ext} the device approaches the interface and the number of l components needed for a correct description increases.

It is straightforward to generalize these results to more complex arrays of point forces, including asymmetric configurations and rotations of the droplet.

VI. CONCLUSIONS AND OUTLOOK

Point forces in the interior of a fluid droplet generate flow and thereby can propel the droplet. By constructing the Green function for the boundary conditions of a fluid droplet, we were able to compute the linear and rotational velocities of the droplet as a function of general point force configurations.

Starting from a single point force, we showed that the translational mobility of the droplet is anisotropic: $v^i_{\text{cm}} = \mu_t^{ij}(\boldsymbol{r}_0)F^j$. The rotational motion of the droplet is determined by the torque of the device with respect to the center of the droplet, i.e., $\boldsymbol{r}_0 \times \mathbf{F}$, and the rotational mobility is isotropic but potentially nonmonotonic as a function of the position of the device. Considering stepwise more complex configurations, we next discussed force dipoles, which in general give rise to both translational and rotational motion of the droplet. Force dipoles include as special cases stresslets as a simple model for an autonomous device as well as rotlets as an approximation for externally driven, helical swimmers. A more refined model of an autonomous device includes three point forces, such that both the total force and torque vanish. The translational velocity of the droplet is independent of the position of the device if the total force dipole moment vanishes.

We have also considered general force distributions and have shown that the propulsion velocities of the droplet depend only on a few multipole moments of the force. The translational velocity is determined by the total force, dipole moment, and quadrupole moment. The rotational velocity requires an additional special octupole moment. Therefore different force distributions give rise to the same propulsion of the droplet, provided these low order moments are the same.

For many applications, such as medical microrobotics, it is desirable to control the trajectory of the forcing device, such that a prescribed trajectory of the droplet results. Approximating the device by a small spherical bead allows us to use Stokes's law supplemented by Faxén's law to derive an approximate relation between the velocity of the device and the applied forces. To illustrate our approach, we consider two illustrative examples: a single bead dragged by an external force and a biflagellate swimmer modeled as a stresslet. The latter allows for a steady comoving state of the droplet and the device. Depending on the position of the device within the droplet, we find two stable fixed points for the relative velocity and finite propulsion. The two stable fixed points are separated by an unstable one, where the device is located at the center of the droplet and no propulsion occurs. If the biflagellate swimmer is additionally controlled by a tiny external steering force, one of the fixed points is selected, allowing for a switch between forward and backward motion.

Alternatively one might consider a squirmer in a droplet, possibly driven by an external force in addition to the autonomous activity. Thereby the trajectory of the squirmer as well as of the droplet could be controlled, generalizing the work of [20]. First results along this line have been published [29].

Note added. Recently, Sprenger *et al.* [30] submitted a paper with some overlap with our paper. Both papers consider the propulsion of a droplet driven by point forces but use different methods of solution. Furthermore, we consider general configurations of point forces and include chiral flow, giving rise to rotational motion of the droplet. We also discuss the possibilities of a stationary state in which a droplet and a device move with the same velocity. Sprenger *et al.* on the other hand discuss a surfactant laden droplet and its effects on the dynamics of the encapsulated swimmer.

APPENDIX A: NONCHIRAL FLOW IN THE INTERIOR OF THE DROPLET

In this Appendix, we construct the nonchiral flow components v_{lm0} and v_{lm1} due to a point force in the interior of the droplet. The solutions of the homogeneous equation are given by

$$v_{lm0}^{\mathrm{hom}}(r) = a_{lm}^{-}\left(\frac{r}{R}\right)^{\ell+1} + b_{lm}^{-}\left(\frac{r}{R}\right)^{\ell-1}, \tag{A1}$$

$$v_{lm1}^{\mathrm{hom}}(r) = \frac{3+\ell}{\ell(\ell+1)}a_{lm}^{-}\left(\frac{r}{R}\right)^{\ell+1} + \frac{1}{\ell}b_{lm}^{-}\left(\frac{r}{R}\right)^{\ell-1}. \tag{A2}$$

We need to find a special solution of the inhomogeneous equation. Our starting point is Eq. (25) in the main text, which we recall here for convenience:

$$\eta\left(\frac{d^2}{dr^2} + \frac{4}{r}\frac{d}{dr} + \frac{2-l(l+1)}{r^2}\right)v_{lm0} = \frac{\ell}{r}A_{lm}\left(\frac{r}{R}\right)^{\ell}\Theta(r_0-r) - \frac{\ell+1}{r}B_{lm}\left(\frac{R}{r}\right)^{\ell+1}\Theta(r-r_0). \tag{A3}$$

Special solutions of this equation are $r^{\ell+1}$ for the inner sphere and $r^{-\ell}$ for the outer shell, suggesting an ansatz $v_{lm0}^{\mathrm{inh}}(r) = C_{lm}^{-}(r/R)^{\ell+1}\Theta(r_0-r) + C_{lm}^{+}(R/r)^{\ell}\Theta(r-r_0)$. However, the flow and its derivative have to be continuous at r_0. Continuity can be achieved by adding solutions of the homogeneous equation, $r^{\ell-1}$, $\ell \geqslant 1$ for the flow in the inner sphere and $r^{-\ell-2}$ for the outer shell. Combining all these terms leads us to the following ansatz:

$$\begin{aligned}\frac{1}{R}v_{lm0}^{\mathrm{inh}}(r) = {} & C_{lm}^{-}\left(\frac{r}{R}\right)^{\ell+1}\Theta(r_0-r) + C_{lm}^{+}\left(\frac{R}{r}\right)^{\ell}\Theta(r-r_0) \\ & + F_{lm}\left(\frac{r}{R}\right)^{\ell-1}\Theta(r_0-r) + H_{lm}\left(\frac{R}{r}\right)^{\ell+2}\Theta(r-r_0).\end{aligned} \tag{A4}$$

When plugged into Eq. (A3), all four sets of coefficients are determined in terms of f_{lm0} and f_{lm1}:

$$\begin{aligned}C_{lm}^{-} &= \frac{\ell}{4\ell+6}\frac{A_{lm}}{\eta^{-}}, \quad C_{lm}^{+} = \frac{\ell+1}{4\ell-2}\frac{B_{lm}}{\eta^{-}}, \quad F_{lm} = \frac{2C_{lm}^{+}}{2\ell+1}\left(\frac{R}{r_0}\right)^{2\ell-1} - \frac{2\ell+3}{2\ell+1}C_{lm}^{-}\left(\frac{r_0}{R}\right)^{2}, \\ H_{lm} &= -\frac{2\ell-1}{2\ell+1}C_{lm}^{+}\left(\frac{r_0}{R}\right)^{2} - \frac{2}{2\ell+1}C_{lm}^{-}\left(\frac{r_0}{R}\right)^{2\ell+3}.\end{aligned} \tag{A5}$$

The coefficients A_{lm} and B_{lm} are given in terms of f_{lm0} and f_{lm1} in Eqs. (23) and (24). The constraint of incompressibility determines v_{lm1}^{inh} from Eq. (19).

The special solution of the inhomogeneous equation is simply related to the Oseen tensor with Cartesian components G_{ij}:

$$v_i(\mathbf{r}\,|\,\boldsymbol{r}_0) = \sum_j G_{i,j}(\boldsymbol{r}\,|\,\boldsymbol{r}_0)F_j \tag{A6}$$

where we have made the dependence of $\mathbf{v}$ on $\mathbf{r}_0$ explicit again. Inserting its expansion in vector spherical harmonics,

$$G_{ij}(\mathbf{r},\mathbf{r}_0) = \sum_{s,s'}\sum_{lm} G_{lm}^{s,s'}(r,r_0)\left[\mathbf{Y}_{lm}^{(s)}(\Omega)\right]_i\left[\mathbf{Y}_{lm}^{*(s')}(\Omega_0)\right]_j,$$

into Eq. (A6) yields

$$v_{lms}(r,\mathbf{r}_0) = \sum_{s'} G_{lm}^{s,s'}(r,r_0)f_{lms'}(\Omega_0)\frac{1}{A_l^{(s')}}.$$

The chiral component ($s=2$) decouples and is solely determined by the special solution of the inhomogeneous equation v_{lm2}^{inh}, constructed in Sec. III C:

$$\sqrt{\ell(\ell+1)}G_{lm}^{2,2}(r,r_0) = -\frac{1}{\eta^{-}(2\ell+1)}\left(\Theta(r-r_0)\frac{r_0^{\ell}}{r^{\ell+1}} + \Theta(r_0-r)\frac{r^{\ell}}{r_0^{\ell+1}}\right).$$

The other components require the inversion of a 2×2 matrix, which is not needed here.

Having constructed a special solution to the inhomogeneous equation, one can now simply add the homogeneous flow fields to obtain the general solution and match the boundary conditions, which is explained in the next section.

APPENDIX B: MATCHING BOUNDARY CONDITIONS

The flow outside of the droplet is given by the homogeneous solutions

$$v^+_{lm0}(r) = a^+_{lm}\left(\frac{R}{r}\right)^{\ell} + b^+_{lm}\left(\frac{R}{r}\right)^{\ell+2}, \tag{B1}$$

$$v^+_{lm1}(r) = \frac{2-\ell}{\ell(\ell+1)} a^+_{lm}\left(\frac{R}{r}\right)^{\ell} - \frac{1}{\ell+1} b^+_{lm}\left(\frac{R}{r}\right)^{\ell+2}, \tag{B2}$$

while the flow in the inside is given by the superposition of the inhomogeneous and homogeneous flow. The boundary conditions determine the four yet unknown coefficients $a^{\pm}_{lm}$ and $b^{\pm}_{lm}$ of the homogeneous flow: two linear equations emerging from the continuity of the flow velocity at $r = R$, and another set of two linear equations emerging from the balance of forces on the surface of the droplet, $\mathbf{e}_r \cdot (\boldsymbol{\sigma}_+ - \boldsymbol{\sigma}_-) = (2\gamma_0/R)\mathbf{e}_r$.

The boundary condition that the flow is continuous gives rise to two equations, corresponding to v_{lm0} and v_{lm1}:

$$a^+_{lm} + b^+_{lm} = a^-_{lm} + b^-_{lm} + R(C^+_{lm} + H_{lm}), \tag{B3}$$

$$(2-l)a^+_{lm} - l b^+_{lm} = (l+3)a^-_{lm} + (l+1)b^-_{lm} + R(2-l)C^+_{lm} - lRH_{lm}. \tag{B4}$$

The boundary condition that the surface of the droplet is force free requires the calculation of the tractions $\boldsymbol{t}^{\pm} = \boldsymbol{e}_r \cdot \boldsymbol{\sigma}^{\pm}$ as an expansion in vector spherical harmonics. The expansion coefficients t_{lms} are related to those of the velocity [24]

$$t_{lm0}(r) = \left(-p_{lm}(r) + 2\eta \tfrac{dv_{lm0}}{dr}\right), \quad t_{lm1}(r) = \eta\left(\frac{dv_{lm1}}{dr} - \frac{v_{lm1}}{r} + \frac{v_{lm0}}{r}\right)$$

for both the external and the internal flow. The surface tension γ_0 is balanced by the $\ell = 0$ component of the pressure, so that the force-free condition reads $t^+_{lm0}(R) = t^-_{lm0}(R)$ and $t^+_{lm1}(R) = t^-_{lm1}(R)$ for $\ell \geqslant 1$. These two boundary conditions provide two more equations for the coefficients:

$$\begin{aligned} &2\frac{l^2+3l-1}{l+1}a^+_{lm} + 2(l+2)b^+_{lm} + \frac{2\lambda}{l}(l^2-l-3)a^-_{lm} + 2\lambda(l-1)b^-_{lm} \\ &\quad = \frac{R}{\eta^+}B_{lm} + 2\lambda R[C^+_{lm} + (l+2)H_{lm}], \end{aligned} \tag{B5}$$

$$\begin{aligned} &2(l^2-1)a^+_{lm} + 2l(l+2)b^+_{lm} - \lambda 2l(l+2)a^-_{lm} - 2\lambda(l^2-1)b^-_{lm} \\ &\quad = 2\lambda R(l^2-1)C^+_{lm} + 2\lambda Rl(l+2)H_{lm}. \end{aligned} \tag{B6}$$

The four equations (B3)–(B6) determine the coefficients of the homogeneous solutions and are conveniently written in matrix notation for the vector of coefficients $\mathbf{Z} = (a^+_{lm}, b^+_{lm}, a^-_{lm}, b^-_{lm})^t$. In this notation the system of four equations resulting from the four boundary conditions is written in compact form as $\hat{\mathbf{M}}\mathbf{Z} = \mathbf{I}$ with

$$\hat{\mathbf{M}} = \begin{pmatrix} 1 & 1 & -1 & -1 \\ \frac{2-l}{l(l+1)} & \frac{-1}{l+1} & -\frac{l+3}{l(l+1)} & -\frac{1}{l} \\ 2\frac{l^2+3l-1}{l+1} & 2(l+2) & \frac{2}{l}\lambda(l^2-l-3) & 2\lambda(l-1) \\ 2(l^2-1) & 2l(l+2) & -2\lambda l(l+2) & -2\lambda(l^2-1) \end{pmatrix}$$

and the vector $\mathbf{I} = (I_{lm}^{(1)}, I_{lm}^{(2)}, I_{lm}^{(3)}, I_{lm}^{(4)})^t$:

$$\mathbf{I} = \begin{pmatrix} RC_{lm}^{+} + RH_{lm} \\ \frac{2-l}{l(l+1)} RC_{lm}^{+} - RH_{lm}/(l+1) \\ \frac{R}{\eta^{+}} B_{lm} + 2\lambda RlC_{lm}^{+} + 2\lambda R(l+2)H_{lm} \\ 2\lambda R(l^2-1)C_{lm}^{+} + 2\lambda Rl(l+2)H_{lm} \end{pmatrix}. \tag{B7}$$

The solution, $a_{lm}^{\pm}, b_{lm}^{\pm}$, is obtained from $\hat{\mathbf{M}}^{-1}\mathbf{I}$ with the help of symbolic machine computation or numerical evaluation, except for the special case $\ell = 1$, discussed below.

APPENDIX C: PROPULSION VELOCITIES

The propulsion velocities require only the $\ell = 1$ component of the flow (9) and (10). Since the linear equations, $\hat{\mathbf{M}}\mathbf{Z} = \mathbf{I}$, for the coefficients $\mathbf{Z} = (a_{lm}^{+}, b_{lm}^{+}, a_{lm}^{-}, b_{lm}^{-})^t$ are decoupled for different ℓ, it is sufficient to consider the case $\ell = 1$, for which the matrix $\hat{\mathbf{M}}$ simplifies considerably. The coefficients are given explicitly by

$$a_{1m}^{+} = \left(I_{1m}^{(3)} - I_{1m}^{(4)}\right)/3, \tag{C1}$$

$$b_{1m}^{+} = \frac{I_{1m}^{(4)} + 6\lambda\left(I_{1m}^{(1)} - I_{1m}^{(2)} - a_{1m}^{+}/2\right)}{3(2+3\lambda)}. \tag{C2}$$

These coefficients determine $\mathbf{v}_{CM}$ according to Eq. (9), which is most easily evaluated with help of the external flow field:

$$\boldsymbol{v}_{CM} = \frac{3}{4\pi} \sum_m \int_{\partial V} d\Omega \, (a_{1m}^{+} + b_{1m}^{+}) Y_{1m}(\Omega) \mathbf{e}_r. \tag{C3}$$

The simplest case is a force $\mathbf{F} = F\boldsymbol{e}_z$ parallel to $\mathbf{r}_0 = z_0\boldsymbol{e}_z$, so that only $m = 0$ contributes: $f_{100} = \sqrt{\frac{3}{4\pi}} F$. The linear propulsion velocity is then given by

$$\boldsymbol{v}_{CM} = \boldsymbol{e}_z \sqrt{\frac{3}{4\pi}} (a_{10}^{+} + b_{10}^{+}) = \frac{\mathbf{F}}{4\pi\eta^{-}R} \frac{3 + 2\lambda - \left(\frac{z_0}{R}\right) z_0^2}{2+3\lambda}. \tag{C4}$$

For a general direction of the force the following relations are used to express the expansion coefficients f_{1ms} in coordinate-free form:

$$\mathbf{F} \cdot \boldsymbol{Y}_{10}^{0} = \sqrt{\frac{3}{4\pi}} \mathbf{F}_{||} \cdot \boldsymbol{e}_z, \tag{C5}$$

$$\mathbf{F} \cdot \boldsymbol{Y}_{10}^{1} = \sqrt{\frac{3}{4\pi}} (\mathbf{F} - \mathbf{F}_{||}) \cdot \boldsymbol{e}_z, \tag{C6}$$

$$\mathbf{F} \cdot \boldsymbol{Y}_{11}^{0} = -\sqrt{\frac{3}{8\pi}} \mathbf{F}_{||} \cdot (\boldsymbol{e}_x + i\boldsymbol{e}_y), \tag{C7}$$

$$\mathbf{F} \cdot \boldsymbol{Y}_{11}^{1} = -\sqrt{\frac{3}{8\pi}} (\mathbf{F} - \mathbf{F}_{||}) \cdot (\boldsymbol{e}_x + i\boldsymbol{e}_y), \tag{C8}$$

$$\mathbf{F} \cdot \boldsymbol{Y}_{10}^{2} = -\sqrt{\frac{3}{4\pi}} \frac{\boldsymbol{r}_0 \times \mathbf{F}}{r_0} \cdot \boldsymbol{e}_z, \tag{C9}$$

$$\mathbf{F} \cdot \boldsymbol{Y}_{11}^{2} = \sqrt{\frac{3}{8\pi}} \frac{\boldsymbol{r}_0 \times \mathbf{F}}{r_0} \cdot (\boldsymbol{e}_x + i\boldsymbol{e}_y) \tag{C10}$$

where $\mathbf{F}_{||} = (\mathbf{F}\cdot\boldsymbol{r}_0)\boldsymbol{r}_0/r_0^2$. The expansion coefficients of the force f_{1m0} and f_{1m1} determine the expansion coefficients $A_{lm}, B_{lm}, C^-_{lm}, C^+_{lm}, F_{lm}, H_{lm}$ [Eqs. (23) and (A5)] and hence the flow field for general force. The final step is the computation of the propulsion velocity from Eq. (C3) with the result given in the main text [Eq. (26)].

Once the flow field of a single point force is known, a general assembly of point forces can be treated by superposition. An example is the force dipole $\boldsymbol{f} = \mathbf{F}\delta(\boldsymbol{r}-\boldsymbol{r}^+) - \mathbf{F}\delta(\boldsymbol{r}-(\boldsymbol{r}^-)$ with $\boldsymbol{r}^\pm = \boldsymbol{r}_0 \pm \mathbf{d}/2$ (see Fig. 2). The propulsion velocities for the dipole are obtained by superposition of the results from Eqs. (26) and (18):

$$\boldsymbol{v}_{\rm cm} = \frac{1}{4\pi\eta^+ R^3(3\lambda+2)}[(\mathbf{F}\cdot\mathbf{d})\boldsymbol{r}_0 + (\mathbf{F}\cdot\boldsymbol{r}_0)\mathbf{d} - 4(\boldsymbol{r}_0\cdot\mathbf{d})\mathbf{F}] \tag{C11}$$

and

$$\boldsymbol{\omega} = -\frac{1}{16\pi\eta^- R^3}\left[\frac{3}{r_0^2}\left(r_0^2+\frac{d^2}{4}\right) - 2\lambda - 3\right](\mathbf{d}\times\mathbf{F}) - \frac{6}{16\pi\eta^- R^4}(\mathbf{r}_0\cdot\mathbf{d})\,(\boldsymbol{r}_0\times\mathbf{F}). \tag{C12}$$

In the main text we discuss two special cases, the stresslet and the rotlet.

[1] J. Li, E.-F. de Avila, W. Gao, L. Zhang, and J. Wang, Micro/nanorobots for biomedicine: Delivery, surgery, sensing, and detoxification, Science Robotics **2**, eaam6431 (2017).

[2] C. Hu, S. Pane, and B. J. Nelson, Soft micro- and nanorobotics, Annu. Rev. Control Robot. Auton. Syst. **1**, 53 (2018).

[3] Y. Ding, F. Qiu, X. C. i Solvas, F. W. Y. Chiu, B. J. Nelson, and A. deMello, Microfluidic-based droplet and cell manipulations using artificial bacterial flagella, Micromachines **7**, 25 (2016).

[4] A. Servant, F. Qiu, M. Mazza, K. Kostarelos, and B. J. Nelson, Controlled in vivo swimming of a swarm of bacteria-like microrobotic flagella, Adv. Mat. **27**, 2981 (2015).

[5] A. W. Feinberg, Biological soft robotics, Annu. Rev. Biomed. Eng. **17**, 243 (2015).

[6] M. Kojima, Z. H. Zhang, M. Nakajima, K. Ooe, and T. Fukuda, Construction and evaluation of bacteria-driven liposome. Sens. Actuators B **183**, 395 (2013).

[7] C. Bechinger, R. Di. Leonardo, H. Löwen, C. Reichhardt, G. Volpe, and G. Volpe, Active particles in complex and crowded environments, Rev. Mod. Phys. **88**, 045006 (2016).

[8] C. W. Oseen, *Neuere Methoden und Ergebnisse in der Hydrodynamik* (Akademische Verlagsgesellschaft, Leipzig, 1927).

[9] C. Maul and S. Kim, Image systems for a stokeslet inside a rigid spherical container, Phys. Fluids **6**, 2221 (1994).

[10] C. Maul and S. Kim, Image of point force in a spherical container and its connection to the Lorentz reflection formula, J. Eng. Math. **30**, 119 (1996).

[11] J. Happel and H. Brenner, *Low Reynolds Number Hydrodynamics* (Springer, New York, 1983).

[12] S. Kim and S. J. Karrila, *Microhydrodynamics: Principles and Selected Applications* (Dover, New York, 2005).

[13] Y. O. Fuentes, S. Kim, and D. J. Jeffrey, Mobility functions for two unequal viscous drops in Stokes flow. II. Axisymmetric motion, Phys. Fluids A **1**, 61 (1989).

[14] Y. O. Fuentes, S. Kim, and D. J. Jeffrey, Mobility functions for two unequal viscous drops in Stokes flow. II. Asymmetric motion, Phys. Fluids **31**, 2445 (1988).

[15] A. Chamolly and E. Lauga, Stokes flow due to point torques and sources in a spherical geometry, Phys. Rev. Fluids **5**, 074202 (2020).

[16] A. Daddi-Moussa-Ider, H. Loewen, and S. Gekle, Creeping motion of a solid particle inside a spherical elastic cavity, Eur. Phys. J. E **41**, 104 (2018).

[17] C. Hoell, H. Loewen, M. Menzel, and A. Daddi-Moussa-Ider, Creeping motion of a solid particle inside a spherical elastic cavity. II. Asymmetric motion, Eur. Phys. J. E **42**, 89 (2019).

[18] J. W. Swan and J. F. Brady, The hydrodynamics of confined dispersions, J. Fluid Mech. **687**, 254 (2011).
[19] C. Aponte-Rivera and R. N. Zia, Simulation of hydrodynamically interacting particles confined by a spherical cavity, Phys. Rev. Fluids **1**, 023301 (2016).
[20] S. Y. Reigh, L. Zhu, F. Gallaire, and E. Lauga, Swimming with a cage: Low-Reynolds-number locomotion inside a droplet, Soft Matter **13**, 3161 (2017).
[21] V. A. Shaik, V. Vasani, and A. Ardekani, Locomotion inside a surfactant-laden drop at low surface Peclet number, J. Fluid Mech. **851**, 187 (2018).
[22] B. U. Felderhof and A. Sellier, Mobility matrix of a spherical particle translating and rotating in a viscous fluid confined in a spherical cell, and the rate of escape from the cell, J. Chem. Phys. **254**, 054703 (2012).
[23] R. G. Barrera, G. A. Estevez, and J. Giraldo, Vector spherical harmonics and their application to magnetostatics, European J. Phys. **6**, 287 (1985).
[24] R. Kree, P. S. Burada, and A. Zippelius, From active stresses and forces to self-propulsion of droplets, J. Fluid Mech. **821**, 595 (2017).
[25] V. Mehanda and P. R. Nott, The collective dynamics of self-propelled particles, J. Fluid Mech. **595**, 239 (2008).
[26] R. Dreyfus, J. Baudry, M. L. Roper, M. Fermigier, H. A. Stone, and J. Bibette, Microscopic artificial swimmers, Nature (London) **437**, 862 (2005).
[27] J. Dölger, L. T. Nielsen, T. Kiørboe, and A. Andersen, Swimming and feeding of myxotrophic biflagellates, Sci. Rep. **7**, 39892 (2017).
[28] P. M. Vlahovska, J. Blawzdziewicz, and M. Loewenberg, Small deformation theory for a surfactant-covered drop in linear flow, J. Fluid Mech. **624**, 293 (2009).
[29] R. Kree and A. Zippelius, Controlled locomotion of a droplet propelled by an encapsulated squirmer, Eur. Phys. J. E **44**, 6 (2021).
[30] A. R. Sprenger, V. A. Shaik, A. M. Ardekani, M. Lisicki, A. J. T. M. Mathijssen, F. Guzmán-Lastra, H. Löwen, A. M. Menzel, and A. Daddi-Moussa-Ider, Towards an analytical description of active microswimmers in clean and in surfactant-covered drops, Eur. Phys. J. E **43**, 58 (2020).